SILAR BiOI sensitized TiO2 films for visible light photocatalytic degradation of rhodamine B and 4-chlorophenol

ARTICLE

SILAR BiOI sensitized TiO_2 films for visible light photocatalytic degradation of rhodamine B and 4-chlorophenol

Gylen Odling and Neil Robertson[a]

Abstract: BiOI nanoplates were deposited upon a film of TiO_2 nanoparticles derived from a commercial source using a simple room temperature SILAR method. X-ray diffraction, X-ray photoelectron spectroscopy and electron microscopies have been used to confirm the crystal phase, chemical states of key elements and morphology of the BiOI nanoplate-TiO_2 composites. Using both valence band x-ray photoelectron spectroscopy and UV-vis diffuse reflectance measurements the band structure of the composites is determined to be that of a type II heterojunction. Through initial screening of the photocatalytic activity of the SILAR-modified films it was determined that 5 SILAR cycles was optimal in the photocatalytic degradation of Rhodamine B. The visible light sensitisation effect of BiOI was then proven by examination of the photocatalytic degradation of the colourless organic pollutant 4-chlorophenol showing a large enhancement over an equivalent TiO_2 film.

Introduction

The availability of clean drinking water is becoming a key issue in the modern world[1,2]. Increases in the global population and a concurrent rise in urbanisation and industrialisation is leading to rapidly depleting non-polluted drinking water sources[3]. Advanced oxidation processes (AOP) such as the use of ozone, hydrogen peroxide and ultraviolet (UV) light to generate highly reactive oxidising species (ROS) have been found to be effective in the removal of organic species such as textile pollutants, agricultural and medical wastes from potential drinking water[4,5]. However, the use of chemical reagents and high energy UV light prohibits the widespread use of these methods. Photocatalytic generation of ROS has gained much attention in recent years as a potential method to overcome these issues[6–8]. The most commonly studied material in this area is titanium dioxide (TiO_2)[9,10] which has gained much interest due to its low cost, low toxicity and high stability. Despite these favourable properties, TiO_2 has two drawbacks; firstly, as TiO_2 has a wide band gap (3.0-3.2 eV) the activity of systems based upon this material are fundamentally restricted to UV light and secondly fast recombination of photogenerated electrons and holes means few surface reactions taking place[11]. Much work has been undertaken in this area to improve both the visible light response and charge separation in TiO_2 based photocatalytic materials, such as introduction of dopants[12,13], application of visible active plasmonic metal nanoparticles[14–17] or carbon based nanomaterials[18,19].

One promising method of providing both visible light harvesting and improved charge separation is the combination of TiO_2 with a second, narrower-band-gap material to form a heterojunction[20,21]. TiO_2 is an n-type semiconductor due to the presence of oxygen vacancies in the lattice[22]. Therefore, a heterojunction between a semiconductor of p-type character and TiO_2 forms a p-n junction which has an internal electric field promoting charge separation by driving charges away from one another across the junction[23,24]. By applying a narrow band gap p-type semiconductor we can take advantage this effect and provide visible light sensitisation to give highly efficient visible active photocatalysts. Bismuth oxyiodide (BiOI) is a well-known p-type material with a band gap of approximately 2 eV that can be used as a visible photocatalyst in its own right[25,26], which has been shown to form p-n junctions with n-type materials such as TiO_2[27,28], and as such improve the photoactivity of the material.

Herein we describe the sensitisation of an immobilised film of nanoporous TiO_2 with nanoplates of the narrow band gap p-type material bismuth oxyiodide using a simple sequential ionic layer adsorption and reaction (SILAR) technique. Immobilisation of the TiO_2 film simplifies the separation of the photocatalyst post-use, and reduces the chance that any nanoscale materials will remain in solution – a health risk which has recently been brought to attention in the literature[29,30]. SILAR is ideally suited to modification of films in a simple, controllable manner and has been successfully applied in the field of sensitised solar cells for these reasons[31–33]. For the purposes of photocatalysis SILAR is relatively unexplored and relatively few examples have been reported[34–37]. While BiOI SILAR for photovoltaic applications has been previously studied[38–40], to the best of our knowledge there are no examples of BiOI-TiO_2 heterojunctions formed by SILAR for photocatalytic applications to date. In addition to a full physical and chemical characterisation of the SILAR prepared BiOI-TiO_2 films, we provide experimental evidence for the band structure of the heterojunctions and use this to rationalise the observed photocatalytic properties.

Results and Discussion

Film Fabrication and SILAR Processing

Nanoporous TiO_2 films were formed using commercially available TiO_2 pastes commonly used in the fabrication of dye-sensitised or perovskite solar cells. Upon firing, these pastes give a film of high surface area consisting of an interconnected network of TiO_2

[a] Prof. Neil Robertson
School of Chemistry
University of Edinburgh
Joseph Black Building
David Brewster Road
Edinburgh
United Kingdom
EH9 3FJ
E-mail: n.robertson@ed.ac.uk

Supporting information and open data for this article is given via a link at the end of the document.

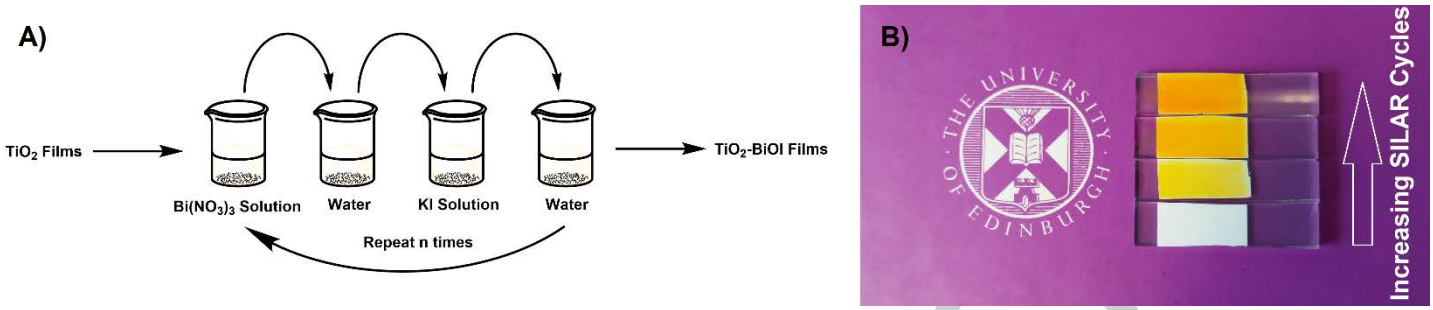

Figure 1. A) The SILAR process used to generate the BiOI-TiO_2 films. B) Digital photograph of the prepared films.

particles to which BiOI SILAR was applied. The typical procedure for BiOI SILAR is given in Figure 1a. During the SILAR processing, the films turned from white to an orange/red colour (Figure 1b), indicating the deposition of BiOI on the surface. Samples will henceforth be named as BiOIxN where N = the number of cycles. Fluorine-doped tin oxide glass substrates were used throughout to improve the films' robustness, as when regular glass was used excessive flaking of the films was observed.

X-Ray Diffraction Analysis

The x-ray diffraction traces of the prepared BiOI-TiO_2 composites are given in Figure 2. Three new peaks of high crystallinity were observed at 2θ values of 29.7°, 33.7° and 45.6°. These can be indexed to the [012], [110] and [020] planes of tetragonal BiOI (JCPDS Card #73-2062). Peaks found at 2θ denoted by blue triangles in Figure 2 were found to be consistent with the anatase phase of TiO_2 (JCPDS Card # 21-1272). Crystallinity has previously been noted to be important in photo-active materials due to raising the diffusion length of excited electrons and holes, leading to improved charge separation in the heterojunction[41,42]. Increased numbers of SILAR cycles were found to increase the intensity of these peaks, indicating the deposition of larger amounts of BiOI.

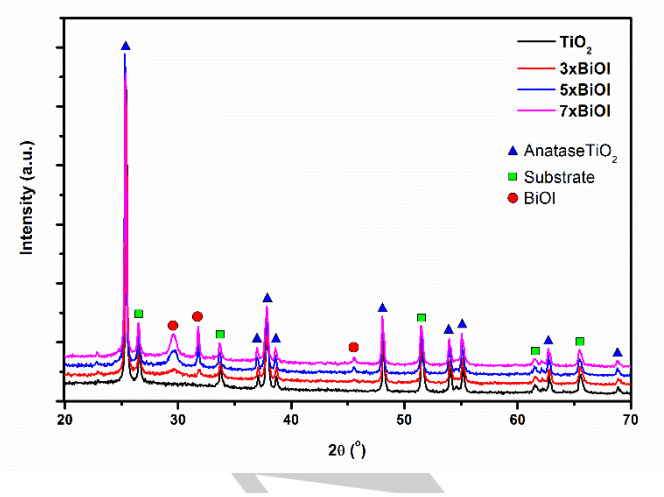

Figure 2. X-ray diffraction traces of the prepared films. Blue triangles denote peaks due to TiO_2, green squares denote peaks due to the FTO substrate and red circles denote peaks due to BiOI.

Scanning and Transmission Electron Microscopy Analysis

Scanning electron microscope (SEM) images of the surface of the prepared films revealed a network of TiO_2 particles of around 150-250 nm with roughly cubic or rod-like morphologies (Figure 3). Upon SILAR cycling BiOI is observed to grow out from the TiO_2 surface with a plate-like morphology, with the plates becoming larger and more prevalent as the number of SILAR cycles is increased. To gain an insight into the films homogeneity below the top layer, cross-sectional SEM images were recorded (Figure S1). The films were all found to be approximately 10 µm thick, with BiOI nanoplates found across the whole cross-section down to the substrate. Transmission electron microscopy (TEM) images of BiOIx5 revealed good contact between the BiOI nanoplates and the TiO_2 particles (Figure S2), with most of the plates being of the order of ~100 nm in length, and around 10-20 nm in width, although shorter plates were also present. TEM elemental maps (Figure 4b,c,d and e) showed that high concentrations of Bi and I were only found in the plates, confirming that these structures are indeed the BiOI formed by SILAR. Selected area electron diffraction (SAED) patterns were also recorded, giving d-spacings of 0.303 and 0.316 nm for the plates (Figure S3), corresponding to the [102] and [312] planes of BiOI respectively[43,44].

Diffuse Reflectance Spectroscopy

BiOI is well known to have an indirect band gap[45–47], and as such the band gap can be obtained from the Tauc plot (Figure 5) according to the following equation:

$$(F(\mathrm{R})h\nu)^{\frac{1}{2}} = A(h\nu - E_g)$$

Where F(R) is the absorption obtained from the Kubelka-Munk function, h is Planck's constant, v is the frequency of the incident light, A is a constant and E_g is the band gap. Extrapolation of the Tauc plot to the x-axis therefore gives the band gaps for the prepared materials, which have been summarised in Table 1. The band gaps of the composites were found to be decrease very slightly as the number of SILAR cycles was increased, while it is clear that the absorption in the visible is improved on repeated SILAR cycling.

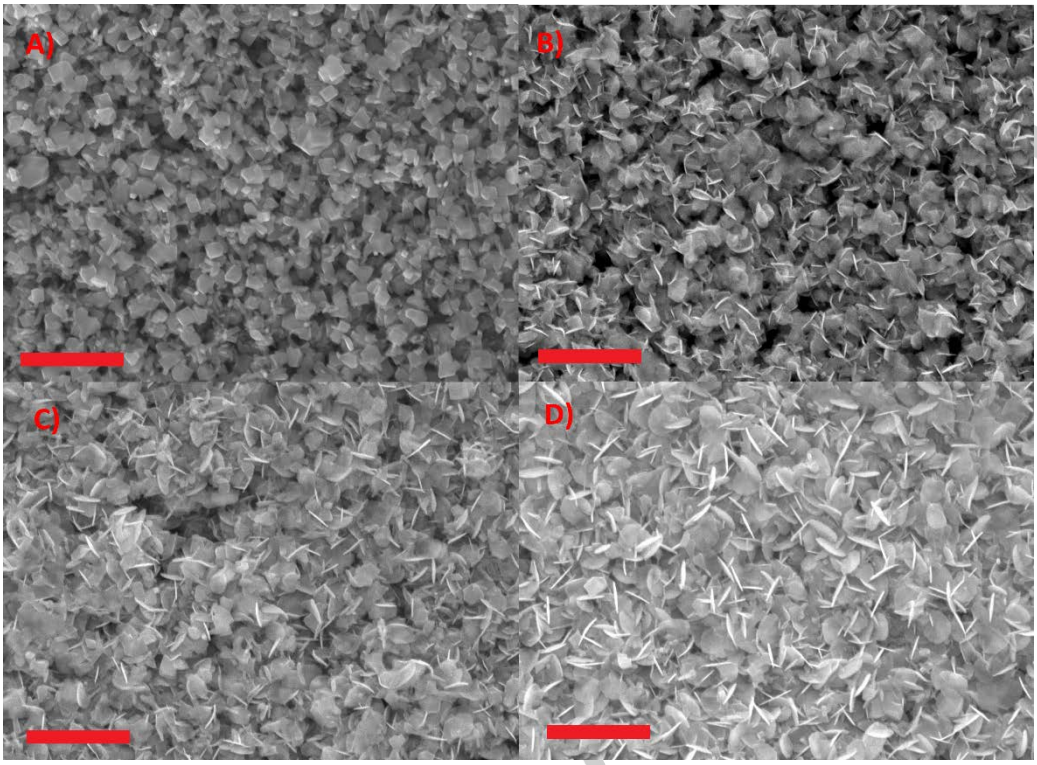

Figure 3. SEM images of A) Blank TiO2 B) 3xBiOI C) 5xBiOI and D) 7xBiOI. Red bar = 1 µm.

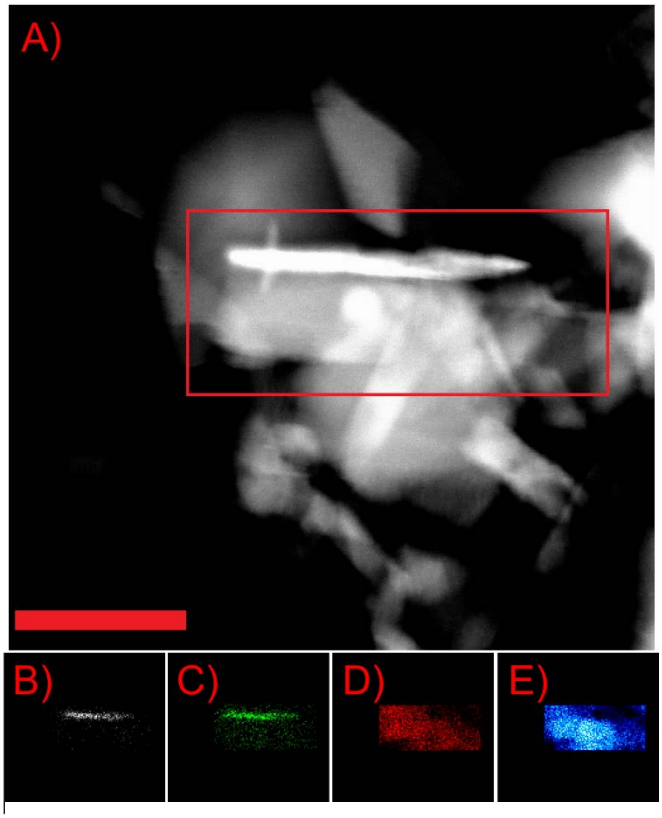

Figure 4. A) Dark field TEM image of a BiOI nanoplate and EDX maps of B) Bi C) I D) O and E) Ti. Red bar = 100 nm, red rectangle denotes area used for elemental mapping.

X-ray photoelectron spectroscopy

The presence of the elements Bi, I, O and Ti were identified in the x-ray photoelectron spectroscopy (XPS) survey scans (Figure S4). In the high resolution (HR-XPS) scan of the 5xBiOI Bi4f region (Figure 6a) showed two peaks at 158.9 eV and 164.2 eV binding energy, corresponding to the $4f_{5/2}$ and $4f_{7/2}$ states of Bi^{3+}. Similarly, the I3d HR-XPS scans (Figure 6b) revealed two peaks at 630.4 eV and 619.0 eV corresponding to the $3d_{1/2}$ and $3d_{3/2}$ peaks of I^-. HR-XPS scans of the Ti 2p and O 2p regions are given in the supporting information (Figures S5). To gain insight into the composite's electronic structure, valence band XPS measurements were also made (Figure 6c) and the results are summarised in Table 1. A large positive shift of ~1.7 eV was noted for the samples modified by SILAR, indicating a raising of the valence band with respect to TiO_2.

Table 1 Valence Band Maxima and Band Gaps

Sample	Valence Band Maxima (eV)	Band Gap (eV)
TiO_2	2.7 ± 0.1	3.26 ± 0.01
3xBiOI	1.0 ± 0.2	2.25 ± 0.01
5xBiOI	1.0 ± 0.0(4)	2.19 ± 0.01
7xBiOI	1.1 ± 0.1	2.14 ± 0.02

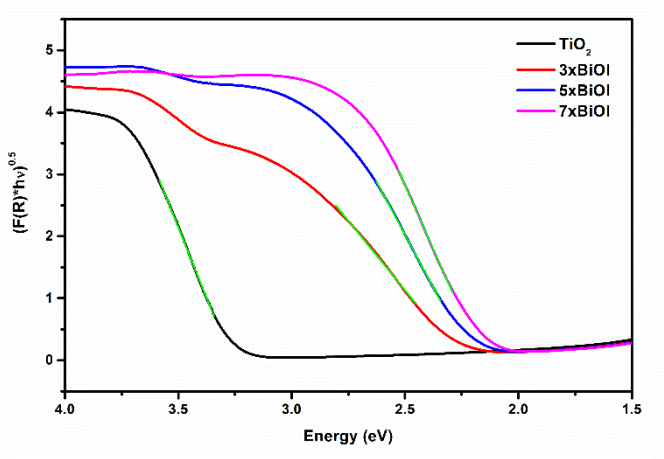

Figure 5. Tauc plots of the prepared composites. Green lines indicate the linear sections used to calculate the band gap.

Band Alignment and Mechanism

Starting from the TiO_2 band gap of 3.2 eV it is possible to construct a band alignment diagram for the composites using the valence band maxima and band gaps determined by diffuse reflectance according to the equation below.

$$E_{cb} = E_{vb} + E_g$$

Where E_{cb} is the conduction band minimum, E_{vb} is the valence band maximum and E_g is the band gap determined from the diffuse reflectance measurement. As found by the valence band XPS measurements, the BiOI valence band lies 1.7 eV above that of TiO_2, and hence the conduction band minimum lies at a value of (1.7 + E_g) above the TiO_2 valence band. Applying this method gives the conduction band of BiOI around 0.7 eV above that of TiO_2 as shown in Figure 7. Therefore, electrons excited by visible light incident upon BiOI have a 0.7 eV driving force to separate from their corresponding holes by transport across the TiO_2-BiOI interface. In a similar fashion, any UV-generated holes in TiO_2 would have a 1.7 eV driving force to migrate to BiOI. This arrangement of the bands is in agreement with the previously suggested alignment formed by equilibration of the Fermi levels of BiOI and TiO_2 when the p-n heterojunction is formed[27,48]. This heterojunction has been recently shown by scavenging experiments carried out by Luo et al[56] to degrade organic species via the formation of the superoxide and hydroxyl radicals under visible light as shown in Figure 7. The formation of a p-n junction is advantageous in driving photoexcited electrons and holes away from one another at the interface between two materials, improving charge separation and therefore photocatalytic activity. As such we have established that the energetics of the BiOI-TiO_2 heterojunction allows both the absorption of visible light, and a mechanism for charge separation across the interface.

Photoluminescence

Photoluminescence measurements are often used to indirectly estimate the degree of charge recombination in heterojunction materials[49]. As photoluminescence arises from radiative recombination of photoexcited holes and electrons, a highly photoluminescent material indicates a high degree of charge recombination. The photoluminescence spectra of the prepared materials excited at 300 nm are given in Figure 8. A large broad peak in the region of 350-550 nm was observed for unaltered TiO_2, where in the SILAR modified samples the peak became almost entirely quenched. This indicates a reduction in charge recombination due to the p-n junction providing good charge separation.

Photocatalytic Testing

Initial photocatalytic screening was carried out by following the photobleaching of the dye Rhodamine B (RhB). Using a standard quartz cuvette as a reactor, the films were placed in the RhB solution and allowed to reach an adsorption-desorption equilibrium (Figure S6). The films were there irradiated using a white LED fitted with a 400 nm filter (emission spectrum: Figure S7) and the pseudo 1st order rate plots are shown in Figure 9a. From these plots it is simple to ascertain the 1st orders rate constants according to the rate equation shown below.

$$-\ln\left(\frac{C}{C_0}\right) = kt$$

Where C is the concentration of the analyte molecule at time t, C_0 is the initial concentration of the analyte, k is the first order rate constant and t is time. According to this equation, the 1st order

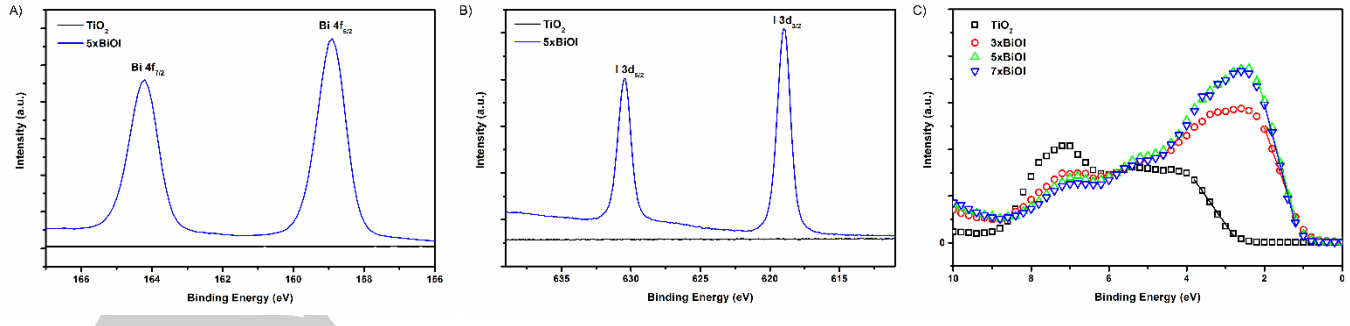

Figure 6. A) HR-XPS of the Bi^{3+} region B) HR-XPS of the I^- region C) HR-XPS of the valence band region with fits of the linear region.

rate constants for the photocatalytic decomposition of RhB are given in table 2.

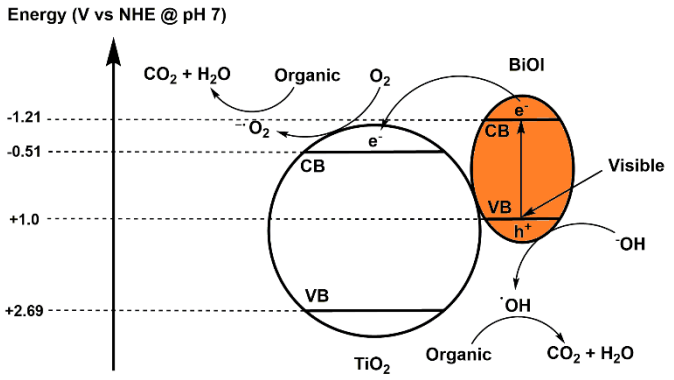

Figure 7. Band structure of the prepared composites, with a proposed mechanism of action.

Table 2 Photocatalytic decomposition of RhB and 4CP

Sample	1st order rate constant (10^{-3} min^{-1})	
	RhB	4CP
No catalyst	0.27	-
TiO_2	2.42	0.09 ± 0.14
3xBiOI	7.57	-
5xBiOI	23.9	3.47 ± 0.05
7xBiOI	19.0	-

It was observed that the composite photocatalytic rates increased as the number of SILAR cycles increased up to 5xBiOI, at which point no further increase was observed and in fact a small decrease was found. This could be due to the BiOI nanoplates becoming too large for charges to effectively inject into the TiO_2 conduction band, or the number of plates could perhaps be hindering the surface of the TiO_2 from the solution. It is noteworthy that as a visible absorbing dye, RhB can photosensitise semiconductors to visible light[50] and as such increase the observed photocatalytic rate. This process, known as self-sensitisation is often overlooked in the literature but can be very significant, indeed in our previous work we found that it can be the difference between a functioning and non-functioning photocatalyst[51]. Hence the rates obtained by studies carried out on visible absorbing dyes under visible irradiation should always be accompanied by a study of a non-excited model organic. In view of this, the best photocatalyst film (5xBiOI) was selected from this initial screening for further testing upon the photobleaching of the UV only absorbing organic pollutant 4-chlorophenol (4-CP) (Figure 9b). The initial 1st order rate constants achieved for 5xBiOI and TiO_2 are compared in Table 2. While a similar trend is observed in the activity of the 3x, 5x and 7xBiOI sensitised films (Figure S8), the photoactivity of 5xBiOI on 4CP is lower than the same material tested on RhB, attributed to the loss of self-sensitisation. However, the lack of this effect means that the rate constant achieved for the degradation of 4CP is a much more accurate reflection of the photocatalytic efficiency of BiOI-TiO_2 towards real-world pollutants. In comparison to photocatalytic BiOI-TiO_2 materials which have been reported previously, the

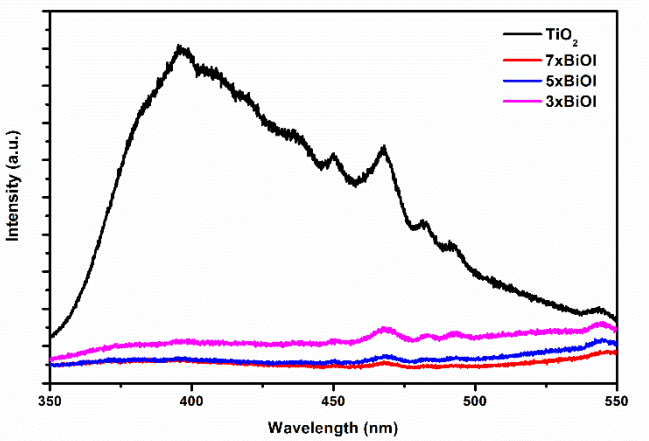

Figure 8. Photoluminescence spectra of the prepared composites and pristine TiO_2 when excited at 350 nm.

SILAR produced material presented here compares very favourably (Table 3). We would emphasise that direct numerical comparison between these different studies cannot be made since all were performed under different conditions, however a broad qualitative comparison is worthwhile to understand the context of our findings. We note that our study was performed using an immobilised film suitable for practical recycling and used a much lower-power light source than the other studies. Despite this, 5xBiOI performs either similarly or better than the previously reported materials in the photocatalytic degradation of dyes. Furthermore, to the best of our knowledge no literature precedent for the photocatalytic degradation of colourless pollutants by BiOI-TiO_2 exist, and as such no comparison could be made for the photodegradation of 4CP. As stated previously, the degradation of colourless organics is a better reflection of a materials activity than that of dyes when using visible light, however this has clearly been overlooked for BiOI-TiO_2 composites. We therefore suggest that this work represents the first accurate reflection of the non-self-sensitised activity of BiOI-TiO_2. A key advantage of the photocatalyst being immobilised as a film is the ability to easily separate and re-use the film without the need to filter nanoparticulate material. Hence, this enabled the long-term stability of the films to be assessed by increasing the irradiation time to 4 hours per run and measuring the degradation efficiency (DE) of 5xBiOI on 4CP upon successive recycles (Figure 10). Degradation efficiency is determined as shown below.

$$DE = \left(1 - \frac{C}{C_0}\right) \times 100$$

Where DE is degradation efficiency as a percentage and both C and C_0 are as defined previously. It was found that ~45% of the 4CP was degraded in the first 4 hours, but that after the first recycle around half the activity was lost. The activity losses however, became smaller on subsequent recycles. There remained a downward trend in the degradation efficiency up to the 20 hours of irradiation tested. It has been noted that BiOI may be somewhat unstable in water due to the loss of iodine and formation of surface hydroxides[55]. The formation of a surface layer of bismuth hydroxide reduces the visible activity as bismuth

hydroxide has no visible absorption, and hence this is a likely reason for the activity losses observed. To probe the changes that occur during photocatalytic testing, X-ray diffraction studies were carried out before and after irradiation (Figure 11). Focusing upon

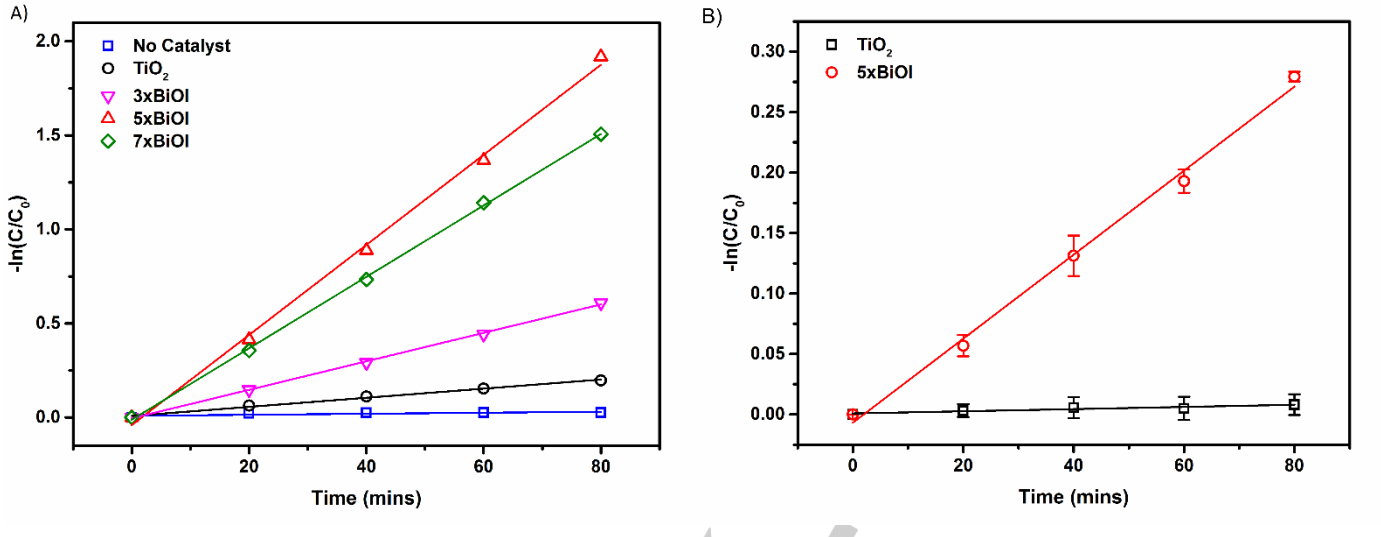

Figure 9. Photocatalytic screening of the prepared photocatalysts upon the degradation of RhB B) Photocatalytic degradation of 4CP using 5xBiOI and TiO_2.

Table 3 Previously reported BiOI-TiO_2 photocatalysts

Preparation	Light Source (filter)	Analyte	Photocatalytic Activity	Reference
Doctor Blading & SILAR	30 W White LED (>400 nm)	Rhodamine B	$23.9*10^{-3}$ min^{-1}	This Work
		4-Chlorophenol	$3.47\pm0.05*10^{-3}$ min^{-1}	
Soft Chemical (80 °C)	500 W Halogen-Tungsten Lamp (>420 nm)	Methyl Orange	1.3925 hr^{-1} ($23.2*10^{-3}$ min^{-1})	Zhang et al[28]
Electrospinning & Hydrothermal	500 W Xe lamp (>420 nm)	Rhodamine B	92 % degradation in 135 mins	Liao et al[52]
Reverse Microemulsion	250 W Halogen Lamp (>420 nm)	Methyl Orange	0.8699 hr^{-1} ($14.5*10^{-3}$ min^{-1})	Liu et al[53]
Electrospinning & Solvothermal	500 W Xe Lamp (>400 nm)	Methylene Blue	0.015 min^{-1}	Zhang et al[54]
Electrospinning & Hydrothermal	500 W Xe Lamp (>420 nm)	Methylene Blue	83 % degradation in 180 mins	Luo et al[56]

the peaks due to the [012] and [110] planes of BiOI at 2θ values of 29.7° and 33.7°, changes in the relative intensities and peak shapes were observed. Generally, both peaks decreased in intensity when compared to the intense anatase peak (blue triangle in Figure 11), indicating a reduction of the concentration or crystallinity of the BiOI. In addition, a distinct change in the shape of the peak corresponding to the [012] plane was noted. Before irradiation a broad symmetric peak was measured, however after irradiation a secondary sharp peak partially overlapping this peak appeared, indicating a secondary phase being present. We tentatively suggest that this secondary phase to be inactive bismuth hydroxide formed during irradiation. Nevertheless, the relatively small losses in activity after the first cycle suggest that further stabilisation of the system might be achievable and this will be the focus of ongoing studies.

Conclusions

We present the formation of BiOI nanoplate sensitised TiO_2 films for the photocatalytic degradation of organic pollutants. SILAR was used as a simple method to grow BiOI at the surface of TiO_2 allowing control of the size and number of BiOI nanoplates, and as such optimise the photocatalytic properties of the film. Using valence band XPS and diffuse reflectance measurements the

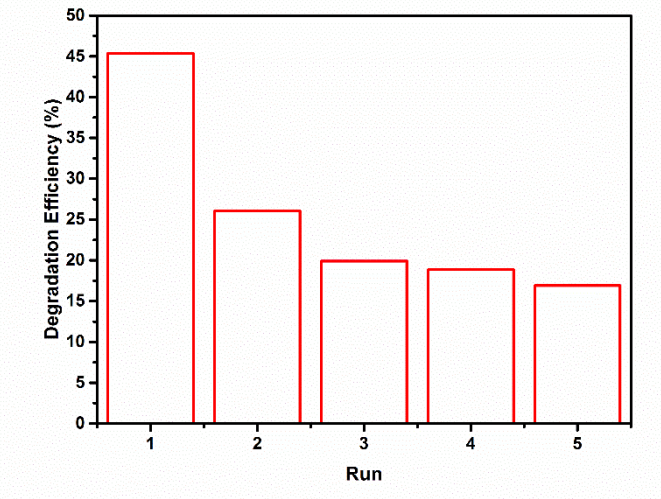

Figure 10. Stability of 5xBiOI upon the photocatalytic degradation of 4CP, where each run is 4 hours of irradiation.

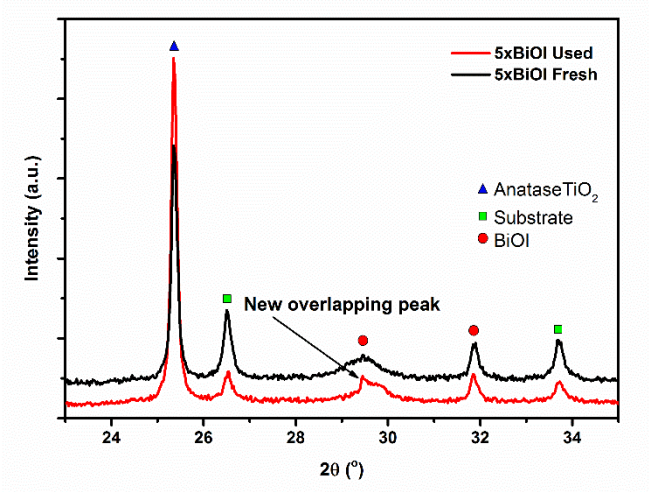

Figure 11. XRD traces of a 5xBiOI film before (black) and after (red) irradiation.

band structure of the composites has been suggested to be that of a type II heterojunction, allowing the migration of excited electrons in BiOI to the TiO_2 conduction band under visible irradiation. This has led the heterojunctions to be effective in the photocatalytic degradation of both the visible active dye RhB and the non-absorbing 4CP under visible light irradiation. Some eventual issues with stability have been uncovered in long term testing, which suggests some further efforts to stabilise the BiOI may be required for the application of this material on a larger scale.

Experimental Section

Chemicals

All reagents were used as received without further purification. Bismuth nitrate pentahydrate (>98%), Potassium Iodide (>99%) 4-chlorophenol (>99%) and Rhodamine B (95%) were purchased from Sigma-Aldrich. The TiO_2 paste was purchased from Dyesol (WER2-O). The FTO glass substrates (TCO30-8) were purchased from Solaronix.

Film preparation

FTO glass substrates were used as a scaffold for the photocatalytic films as it was found that the FTO surface allowed for strongly anchored films, whereas normal glass resulted in the film flaking from the surface. FTO glass was cut into 2cm x 2cm squares before being ultrasonically cleaned in a solution of detergent (Decon 90, ~5% in tap water) for 15 minutes. The substrates were then rinsed with tap water, deionised water and finally ethanol. Titania paste (WER2-O) was then doctor bladed in 1 cm x 2 cm strips onto the surface of the FTO using scotch tape (3M) as a spacer before heating to 510 °C in stages on a controlled hotplate to remove the organic templates, leaving a highly porous TiO_2 film. The temperature profile of the heating regime was as follows: 325 °C for 5 minutes, 375 °C for 5 minutes, 425 °C for 5 minutes, 475 °C for 10 minutes, 510 °C for 10 minutes. The heating ramp rate between each stage was 10 °C min^{-1} apart from the final stage where it slowed to 5 °C min^{-1}. The sintered TiO_2 films were then allowed to cool gradually on the hotplate to room temperature. Narrower (0.9 cm x 2 cm) films were also fabricated in the same way for photocatalytic testing.

SILAR Sensitisation

Aqueous solutions of $Bi(NO_3)_3.5H_2O$ (5 mM) and KI (5 mM) were used as the cation and anion precursors respectively. The as-prepared TiO_2 films were submerged first in the $Bi(NO_3)_3$ solution, then washed with water to remove any loosely bound material before being submerged in the KI solution and finally washed once more with water. This constitutes one full SILAR cycle, and was repeated 3, 5 and 7 times to give differing levels of BiOI on the substrates. 600 second immersions were used for each solution and wash.

Characterisation

UV-visible diffuse reflectance of the films was measured using a JASCO V-670 spectrophotometer with an integrating sphere attachment. Photoluminescence (PL) spectroscopy was carried out on a Horiba Jobin Yvon Fluoromax-3 spectrometer with a fibre optic attachment arranged such that the excitation source was angled at ~45° to the film surface and the detector fibre optic at 90°. PL spectra were measured at room temperature with an excitation wavelength of 300 nm. XPS scans were carried out using a Thermo Scientific Theta Probe XPS with monochromated 1486.6 eV Al Kα irradiation. The C 1s peak due to

adventitious carbon was used as a calibration peak by alignment to 284.8 eV. X-ray diffraction data were acquired on a Bruker D2 phaser model diffractometer using monochromated CuKα radiation. Transmission electron microscope (TEM) images were obtained using a JEOL 2100F FEG TEM operated with an accelerating voltage of 200 kV. SEM images were collected using a Carl Zeiss SIGMA HD VP Field Emission SEM, operated in InLens mode with a 10 kV accelerating voltage. For measurements accompanied by an error range, the error has been calculated on the basis of three measurements.

Photocatalytic testing

Narrow films (0.9 cm x 2 cm) were submerged into a solution of Rhodamine B (2 ml, 10 μmolar) in a quartz cuvette. The films were stirred in the dark for up to 60 minutes to establish an adsorption equilibrium, then irradiated with a white LED (30 W applied power) fitted with a UV filter (>400 nm, Thorlabs). The decolourisation of Rhodamine B was followed by measuring the absorption at 553 nm at regular time intervals using a JASCO V-670 spectrophotometer. The degradation of 4-chlorophenol was measured in the same way, using 4-chlorophenol of 156 μmolar concentration followed using the peak at 280 nm. In the assessment of the recyclability of the films, a single measurement after 4 hours irradiation was taken to calculate the degradation efficiency, between runs the film was washed thoroughly with water and dried under a stream of N_2.

Acknowledgements

X-ray photoelectron spectra were obtained at the National EPSRC XPS Users' Service (NEXUS) at Newcastle University, an EPSRC Mid-Range Facility. This work was funded as part of the CRITICAT Centre for Doctoral Training (Ph.D. studentship to O.G.; grant code: EP/L016419/1).

Supporting Information: _____

Open Data: _____

Keywords: Photocatalysis • TiO_2 • Water • Heterojunction • Photodegradation

[1] United Nations Water, *The United Nations World Water Development Report 2016*, **n.d.**
[2] World Health Organisation, *World Health Organisation Fact Sheet N°372*, **2012**.
[3] United Nations Water, *Water Scarcity*, **2013**.
[4] G. Ruppert, R. Bauer, *Chemosphere* **1994**, *28*, 1447–1454.
[5] Y. Lee, U. von Gunten, *Water Res.* **2010**, *44*, 555–566.
[6] M. Ge, C. Cao, J. Huang, S. Li, Z. Chen, K.-Q. ZHANG, S. S. Al-deyab, Y. Lai, *J. Mater. Chem. A* **2016**, *4*, 6772–6801.
[7] B. Luo, G. Liu, L. Wang, *Nanoscale* **2016**, *8*, 6904–6920.
[8] H. Park, Y. Park, W. Kim, W. Choi, *J. Photochem. Photobiol. C Photochem. Rev.* **2013**, *15*, 1–20.
[9] X. Chen, S. S. Mao, *Chem. Rev.* **2007**, *107*, 2891–2959.
[10] K. Nakata, A. Fujishima, *J. Photochem. Photobiol. C Photochem. Rev.* **2012**, *13*, 169–189.
[11] M. R. Hoffmann, S. T. Martin, W. Choi, D. W. Bahnemannt, *Chem. Rev.* **1995**, *95*, 69–96.
[12] X. Zhou, V. Häublein, N. Liu, N. T. Nguyen, E. M. Zolnhofer, H. Tsuchiya, M. S. Killian, K. Meyer, L. Frey, P. Schmuki, *Angew. Chemie Int. Ed.* **2016**, *55*, 3763–3767.
[13] H. Zeng, J. Xie, H. Xie, B. Su, M. Wang, H. Ping, W. Wang, H. Wang, Z. Fu, *J. Mater. Chem. A* **2015**, *3*, 19588–19596.
[14] J. Zhao, P. Xu, Y. Li, J. Wu, J. Xue, Q. Zhu, X. Lu, W. Ni, *Nanoscale* **2015**, *8*, 5417–5421.
[15] J. Lu, P. Zhang, A. Li, F. Su, T. Wang, Y. Liu, J. Gong, *Chem. Commun. (Camb).* **2013**, *49*, 5817–9.
[16] B. Wu, D. Liu, S. Mubeen, T. T. Chuong, M. Moskovits, G. D. Stucky, *J. Am. Chem. Soc.* **2016**, *138*, 1114–1117.
[17] J. B. Priebe, J. Radnik, A. J. J. Lennox, M. Pohl, M. Karnahl, D. Hollmann, K. Grabow, U. Bentrup, H. Junge, M. Beller, et al., *ACS Catal.* **2015**, *5*, 2137–2148.
[18] H. Li, L. Zhou, L. Wang, Y. Liu, J. Lei, J. Zhang, *Phys. Chem. Chem. Phys.* **2015**, *17*, 17406–17412.
[19] Q. Zhang, Q. An, X. Luan, H. Huang, X. Li, Z. Meng, W. Tong, X. Chen, P. K. Chu, Y. Zhang, *Nanoscale* **2015**, *7*, 14002–14009.
[20] Y. Wang, Q. Wang, X. Zhan, F. Wang, M. Safdar, J. He, *Nanoscale* **2013**, *5*, 8326–39.
[21] J. Li, N. Wu, *Catal. Sci. Technol.* **2015**, *5*, 1360–1384.
[22] B. J. Morgan, G. W. Watson, *J. Phys. Chem. C* **2010**, *114*, 2321–2328.
[23] M. Wang, Y. Hu, J. Han, R. Guo, H. Xiong, Y. Yin, *J. Mater. Chem. A* **2015**, *3*, 20727–20735.
[24] L. Liu, W. Yang, W. Sun, Q. Li, J. K. Shang, *ACS Appl. Mater. Interfaces* **2015**, *7*, 1465–1476.
[25] Y. Wang, K. Deng, L. Zhang, *J. Phys. Chem. C* **2011**, *115*, 14300–14308.
[26] J. Xia, S. Yin, H. Li, H. Xu, Y. Yan, Q. Zhang, *Langmuir* **2011**, *27*, 1200–1206.
[27] Y. Zhang, Q. Pei, J. Liang, T. Feng, X. Zhou, H. Mao, W. Zhang, Y. Hisaeda, X. M. Song, *Langmuir* **2015**, *31*, 10279–10284.
[28] X. Zhang, L. Zhang, T. Xie, D. Wang, *J. Phys. Chem. C* **2009**, *113*, 7371–7378.
[29] T. Tong, C. M. Wilke, J. Wu, C. T. T. Binh, J. J. Kelly, J. F. Gaillard, K. A. Gray, *Environ. Sci. Technol.* **2015**, *49*, 8113–8123.
[30] C. Chen, J. M. Unrine, J. D. Judy, R. W. Lewis, J. Guo, D. H. McNear, O. V. Tsyusko, *Environ. Sci. Technol.* **2015**, *49*, 8759–8768.
[31] Y. Jin-nouchi, S. Naya, H. Tada, *J. Phys. Chem. C* **2010**, *114*, 16837–16842.
[32] H. J. Lee, J. Bang, J. Park, S. Kim, S. M. Park, *Chem. Mater.* **2010**, *22*, 5636–5643.
[33] S. S. Mali, R. S. Devan, Y.-R. Ma, C. A. Betty, P. N. Bhosale, R. P. Panmand, B. B. Kale, S. R. Jadkar, P. S. Patil, J.-H. Kim, et al., *Electrochim. Acta* **2013**, *90*, 666–672.
[34] D. Hou, X. Hu, P. Hu, W. Zhang, M. Zhang, Y. Huang, *Nanoscale* **2013**, *5*, 9764.
[35] W. L. Ong, Y.-F. Lim, J. L. Ting Ong, G. W. Ho, *J. Mater. Chem. A* **2015**, *3*, 6509–6516.
[36] M. Ge, C. Cao, S. Li, S. Zhang, S. Deng, J. Huang, Q. Li, K. Zhang, S. S. Al-Deyab, Y. Lai, *Nanoscale* **2015**, *7*, 11552–11560.
[37] P. Lv, W. Fu, H. Yang, H. Sun, Y. Chen, J. Ma, X. Zhou, L. Tian, W. Zhang, M. Li, et al., *CrystEngComm* **2013**, *15*, 7548–7555.
[38] M. Fang, H. Jia, W. He, Y. Lei, L. Zhang, Z. Zheng, *Phys. Chem. Chem. Phys.* **2015**, *17*, 13531–13538.
[39] K. Wang, F. Jia, Z. Zheng, L. Zhang, *Electrochem. commun.* **2010**, *12*, 1764–1767.
[40] K. Wang, F. Jia, L. Zhang, *Mater. Lett.* **2013**, *92*, 354–357.
[41] W. Zhou, F. Sun, K. Pan, G. Tian, B. Jiang, Z. Ren, C. Tian, H. Fu, *Adv. Funct. Mater.* **2011**, *21*, 1922–1930.
[42] J. B. Joo, Q. Zhang, M. Dahl, I. Lee, J. Goebl, F. Zaera, Y. Yin, *Energy Environ. Sci.* **2012**, *5*, 6321–6327.
[43] S. Huang, Y. Feng, L. Han, W. Fan, X. Zhao, Z. Lou, Z. Qi, B. Yu, N. Zhu, *RSC Adv.* **2014**, *4*, 61679–61686.
[44] S. Chou, C. Chen, Y. Dai, J. Lin, W. William, *RSC Adv.* **2016**, *6*, 33478–33491.
[45] X. Xiao, W.-D. Zhang, *J. Mater. Chem.* **2010**, *20*, 5866.
[46] Y. Lei, G. Wang, S. Song, W. Fan, M. Pang, J. Tang, H. Zhang, *Dalt. Trans.* **2010**, *39*, 3273.
[47] X. Zhang, L. Zhang, *J. Phys. Chem. C* **2010**, *114*, 18198–18206.
[48] Q. Teng, X. Zhou, B. Jin, J. Luo, X. Xu, H. Guan, W. Wang, F. Yang, *RSC Adv.* **2016**, *6*, 36881–36887.
[49] J. Liqiang, Q. Yichun, W. Baiqi, L. Shudan, J. Baojiang, Y. Libin, F. Wei, F. Honggang, S. Jiazhong, *Sol. Energy Mater. Sol. Cells* **2006**, *90*, 1773–1787.
[50] T. Wu, G. Liu, J. Zhao, H. Hidaka, N. Serpone, *J. Phys. Chem. B* **1998**, *102*, 5845–5851.
[51] G. Odling, N. Robertson, *ChemPhysChem* **2016**, 2872–2880.
[52] C. Liao, Z. Ma, G. Dong, J. Qiu, *Appl. Surf. Sci.* **2014**, *314*, 481–489.
[53] Z. Liu, X. Xu, J. Fang, X. Zhu, J. Chu, B. Li, *Appl. Surf. Sci.* **2012**, *258*, 3771–3778.

[54] Y. Zhang, S. Liu, Z. Xiu, Q. Lu, H. Sun, G. Liu, *J. Nanoparticle Res.* **2014**, *16*, 2375.
[55] N. T. Hahn, S. Hoang, J. L. Self, C. B. Mullins, *ACS Nano* **2012**, *6*, 7712–7722.
[56] S. Luo, J. Chen, Z. Huang, C. Liu, M. Fang, *ChemCatChem* **2016**, *8*, 3780–3789